Energies **2015**, *8*, 6328-6349; doi:10.3390/en8076328

OPEN ACCESS

energies

ISSN 1996-1073

www.mdpi.com/journal/energies

Article

Improving Transient Stability in a Grid-Connected Squirrel-Cage Induction Generator Wind Turbine System Using a Fuzzy Logic Controller

Minh Quan Duong [1,2,*], Francesco Grimaccia [1], Sonia Leva [1], Marco Mussetta [1] and Kim Hung Le [2]

[1] Politecnico di Milano, Dipartimento di Energia, Via La Masa 34, 20156 Milano, Italy; E-Mails: francesco.grimaccia@polimi.it (F.G.); sonia.leva@polimi.it (S.L.); marco.mussetta@polimi.it (M.M.)

[2] Department of Electrical Engineering, University of Science and Technology—The University of Da Nang, Block A, 54 Nguyen Luong Bang Street, LienChieu District, DaNang City 59000, Vietnam; E-Mail: lekimhung@dut.udn.vn

* Author to whom correspondence should be addressed; E-Mail: minhquan.duong@polimi.it or dmquan@dut.udn.vn; Tel.: +39-33-8774-7224 or +84-978-468-468.

Academic Editor: Frede Blaabjerg

Received: 28 April 2015 / Accepted: 12 June 2015 / Published: 25 June 2015

Abstract: A common problem in wind power plants involves fixed-speed wind turbines. In fact, being equipped with a squirrel-cage induction generator (SCIG), they tend to drain a relevant amount of reactive power from the grid, potentially causing voltage drops and possible voltage instability. To improve SCIG power quality and transient stability, this paper investigates a new control strategy for pitch angle control based on proportional-integral (PI) controller and a fuzzy logic controller (FLC), considering both normal and fault ride-through (FRT) schemes. In the literature, often, the mechanical torque output is assumed constant for a specific wind speed. This might not be accurate, because the mechanical torque-speed typical of a wind turbine depends also on the power coefficient or pitch angle. In this paper, an analytic model of transient stability is proposed using the equivalent circuit of the SCIG and using the concepts of stable and unstable electrical-mechanical equilibrium. The method has been evaluated by comparing the results obtained by the analytic method with the dynamic simulation. The results show that the proposed hybrid controller is effective at smoothing the output power and complying with FRT requirements for SCIG in the power system.

Keywords: fuzzy logic; wind power; fault ride-through; squirrel-cage induction generator; transient stability

1. Introduction

The increasing demand for energy in the world has forced researchers to explore non-conventional energy and to discover the best solution for exploiting these renewable energy potentials. In particular, recent research activities have been directed toward the development of renewable energy in terms of cost-competitiveness, energy-efficiency and predictability [1,2].

Among these, electricity production from wind turbines (WT) ranks as one of the most assessed alternative energy technologies when it comes to the fulfillment of renewable energy targets set by governments worldwide due to its free, clean and large potential [3]. Nowadays, most of the wind energy conversion systems (WECS) usually employ variable speed wind turbine generation systems (WTGS) [4,5]. However, before the year 2000, WECS were made by fixed-speed induction generators (FSIG), in particular squirrel-cage induction generators (SCIG), which were largely used in power systems because of their reliability, low cost and robustness.

It is well known that SCIGs can generate power fluctuations and stability problems due to their lack of control ability: in fact, reactive power from the grid is required during both normal and fault operation conditions [6]. This can decrease the power quality and cause transient instability [7,8].

Wind power output is proportional to the cube of wind speed, which is time-varying in the real world. Thus, SCIG power fluctuations can lead to over-speed and network instability [9,10].

As a WECS's lifetime is over 20 years, it is still of interest to investigate the interaction of SCIG with the power grid [11]. Consequently, it is important to analyze the impacts of SCIG on the distribution network and to understand the performance of WT under steady-state and transient-state conditions [12].

To the authors' knowledge, little effort has been carried out so far out to analyze the large-disturbance stability of induction generators by using analytic methods. In [12–15], the mechanical torque output of the WT was assumed to be constant, during and after the fault occurrence. This may not be true, because the characteristics of mechanical torque (T_m) depend on the tip speed ratio, (λ) and power coefficient (C_p), which depend on the pitch angle (β), wind speed (V), slip (s) and radius of WT. Our present research shows that the output mechanical torque-speed characteristics of an SCIG depend not only on the wind speed, but also on β. This pitch angle β will change during normal operation and grid faults, which makes the mechanical torque output from the wind turbine nonlinear by our hybrid controller.

Previous research was headed toward the selection of a suitable device for improving SCIG stability problems, such as flexible AC transmission system (FACTS) devices, rotor circuit control, dynamic voltage restorers (DVR) and braking resistors (BR). In [16–19], the effect of FACTS devices is reported to regulate bus voltage and, therefore, to improve the rotor speed stability and voltage fault ride-through (FRT) of the fixed-speed wind generator during and after disturbances. However, solutions based on FACTS are considered expensive [20]. The rotor circuit control is a cost-effective approach used in [14,21,22] for transient stability control. As suggested in [20], a solution is to employ an electronically-controlled external resistance connected to the rotor winding, and another one is to

control the voltage applied to the rotor through a static converter in a doubly-fed induction generator (DFIG) [20]. However, this scheme is only suitable to the wound rotor induction generator and cannot be applied to the SCIG. BR and DVR were introduced as a solution for SCIG stabilization originally in [23], then in [14,24]. The BR decreases the rotor speed and absorbs electrical power during the grid fault, thus improving transient stability. As we can see in [25], this method was already applied for transient stability enhancement of a synchronous generator (SG) in the past. The operation of an asynchronous generator is significantly different from that of an SG, and the BR is less effective for improving the SCIG stability than the SG stability. DVR is a custom power device used to mitigate sags, swells and other power quality issues in power control mode [14]: it is effective for improving the critical clearing time of SCIG-based wind generation. Obviously, all of the previously mentioned methods need additional equipment, such as a static VAR compensator (SVC), static compensator (STATCOM), unified power flow controller (UPFC), DVR, extension resistor and BR, which may not be efficient from the economic point of view.

In a previous work [26], the authors proposed a hybrid control strategy based on proportional-integral (PI) controller and a fuzzy technique for pitch angle control of an SCIG-based WT in order to improve output power quality performance in all of the operating regions. Nevertheless, we did not mention the performance of output power leveling, as well as the SCIG transient process problem. In this paper, the first topic is addressed in Section 5.1; moreover, an analytic method to study the transition process of SCIG is presented in Section 3: this method is based on the steady-state equivalent circuit of the induction generator (IG) and on the the concepts of stable and unstable electrical-mechanical equilibrium points represented in the electrical and mechanical torque *versus* rotor speed space, as suggested in [12]; relative results are reported in Section 5.2.

In previous works, the effectiveness of the hybrid controller with a normal operation scheme was shown to improve the smoothing of output power. In this research, we study the FRT operation scheme to improve the stability characteristics of energy generated from SCIG WT, for several parameters. The paper is organized as follows: in Section 2, the considered mathematical model of SCIG WT is presented; Section 3 presents the new analysis of the SCIG mechanical torque and electrical torque during the transient process; Section 4 proposes a hybrid control design for a pitch angle controller, both for the normal and FRT schemes; in Section 5, the final results are shown and discussed, and the last section reports the conclusions.

2. Model of a Grid-Connected Wind Farm with SCIG

Figure 1 illustrates an SCIG wind farm coupled to a grid at the point of common connection (PCC). Analytic modeling of SCIG WT is well documented in the literature [27–29]. The equivalent circuit of the coupled SCIG with the PCC is shown in Figure 2 [30].

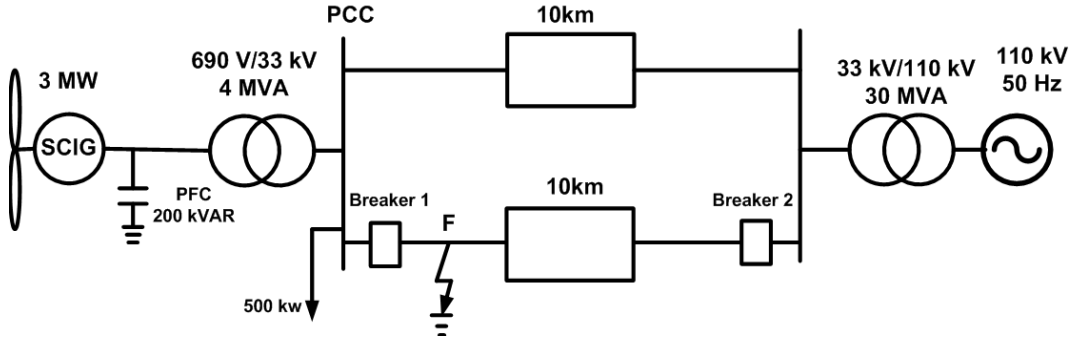

Figure 1. Coupled squirrel-cage induction generator (SCIG)-based wind farm with the point of common connection (PCC).

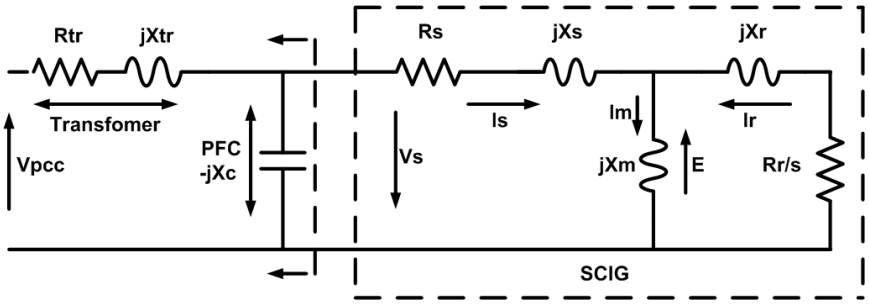

Figure 2. Complete equivalent circuit of a coupled SCIG with the PCC.

2.1. WT Model

The wind turbine rotor converts the kinetic energy absorbed from wind into mechanical power. The available power P_{wt} is:

$$P_{wt} = \frac{1}{2}\rho\pi R^2 V^3 = \frac{1}{2}\rho\pi R^2 (\frac{R}{\lambda})^3 {\omega_R}^3 \tag{1}$$

where ρ is the air density (kg/m^3), R is the blade radius (m), V is the wind speed (m/s), ω_R is the rotor speed (rad/s) and λ is the turbine tip-speed ratio, defined as [31]:

$$\lambda = \frac{\omega_R R}{V} \tag{2}$$

The turbine mechanical power P_{mec} that can be extracted depends on power coefficient C_p or pitch angle β and is given by:

$$P_{mec} = C_p(\lambda,\beta)P_{wt} = \frac{1}{2}C_p(\lambda,\beta)\rho\pi R^2(\frac{R}{\lambda})^3{\omega_R}^3 = C_p(\lambda,\beta)k{\omega_R}^3 \tag{3}$$

$$k = \frac{1}{2}\rho\pi R^2(\frac{R}{\lambda})^3 \tag{4}$$

The mechanical torque output of SCIG WT can be derived as shown in [32]:

$$T_m = \frac{P_{mec}}{\omega_R} = \frac{C_p(\lambda,\beta)P_{wt}}{\omega_R} \tag{5}$$

From the wind turbine characteristics reported in [26], as well as Equation (5), the relationship between the mechanical torque T_m and β is shown in Figure 3. As mentioned in [33], the mechanical torque in Equation (5) is calculated assuming an ideal rotor disk. The turbine speed varies very little due to the steep slope of the generator's torque-speed characteristics; therefore, the mechanical torque depends on $C_p(\lambda, \beta)$. As reported in [33], the typical variation of the tip-speed ratio λ under a 10-second transient simulation is negligible. As a result, the mechanical torque depends on the pitch angle β, as well. In particular, with high rotor speed values, the mechanical torque decreases when the pitch angle is increased, as shown in Figure 3.

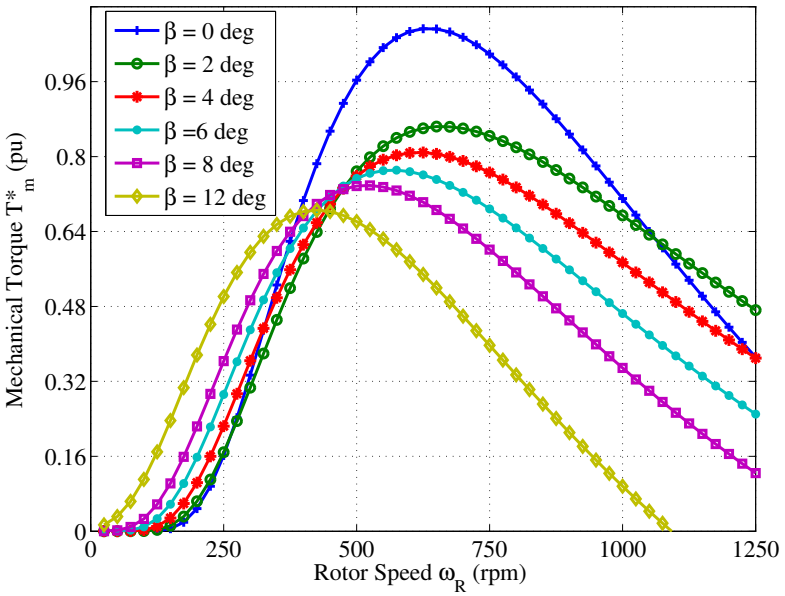

Figure 3. Mechanical torque *versus* rotor speed curve.

2.2. SCIG Model

According to the SCIG static equivalent circuit shown in Figure 2, the voltage equivalent is:

$$E = jI_m X_m = -I_r(R_r/s + jX_r) \tag{6}$$

$$I_m = I_s + I_r \tag{7}$$

$$V_s = E + I_s(R_s + jX_s) \tag{8}$$

$$P_{mec} = 3{I_r}^2(R_r/s) \tag{9}$$

where E is the air gap magnetic field induction electromotive force; I_s, I_r and I_m are the SCIG stator, rotor and exciting current, respectively; R_s and R_r are the stator and rotor resistances; X_s and X_r are the stator and rotor secondary leakage reactances; and X_m is magnetizing reactance. The parameters on the rotor side are converted to the stator side. P_{mec} is also the input generator power; s is the slip ratio, which is less than zero in the dynamo.

Considering the voltage equivalent and a small variation range of s in the real stable [34], we can conclude that:

$$V_s \approx \frac{I_r}{\mid s \mid X_m} k_s \tag{10}$$

where:

$$k_s = \sqrt{M^2 + N^2} \tag{11}$$

$$M = -(sR_sX_r + sR_sX_m + X_sR_r + R_rX_m) \tag{12}$$

$$N = (R_sR_r - sX_rX_s - sX_mX_s - sX_rX_m) \tag{13}$$

Thus, from Equations (3) and (9), we get:

$$I_r = \sqrt{\frac{C_p(\lambda, \beta)k{\omega_R}^3 s}{3R_r}} \tag{14}$$

where s is the slip ratio:

$$s = \frac{\omega_s - \omega_R}{\omega_s} \tag{15}$$

Therefore, from Equations (10), (14) and (15), we get:

$$V_s \approx k_r \sqrt{\frac{{\omega_R}^3}{\mid \omega_s - \omega_R \mid}} \tag{16}$$

where ω_s is the synchronous speed and k_r is defined as:

$$k_r = \frac{k_s\sqrt{\omega_s k C_p(\lambda, \beta)}}{\sqrt{3R_r}X_m} \tag{17}$$

From Equation (16), we can get the behavior of SCIG when ω_R is changing, as reported in Figure 4, which shows that the voltage at the terminal of SCIG is reducing when the rotor speed of WT increases. However, from Equation (17) and Figure 3, we can see that pitch angle β or T_m control, as explained in the next part, is one of the solutions to improve the voltage output of SCIG.

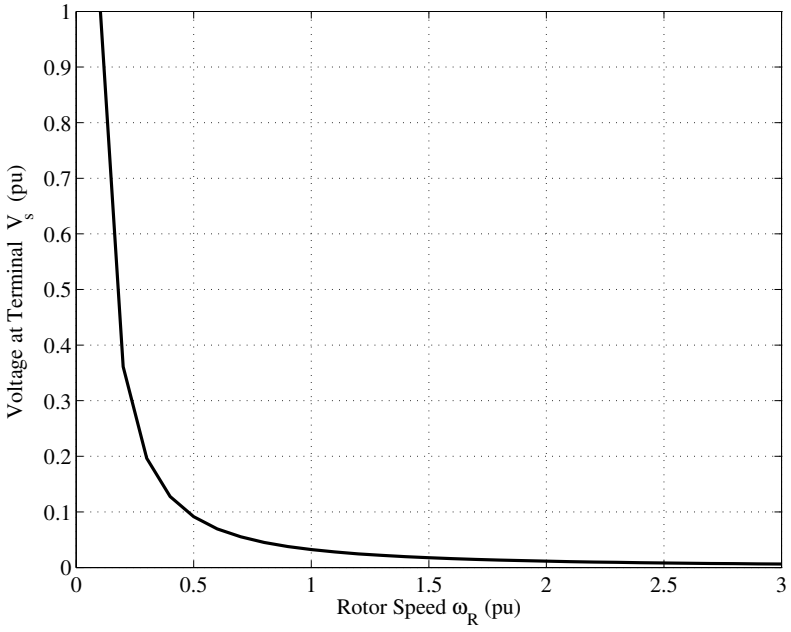

Figure 4. The relationship between voltage and rotor speed in the SCIG interface.

3. Analysis of Transient Stability of SCIG

The test system shown in Figure 1 can be modeled by the equivalent electrical circuit from SCIG to PCC shown in Figure 2. In this figure, V_{pcc} is the PCC voltage phasor, R_{tr} and X_{tr} represent the step-up transformer short-circuit level and X_c is the capacitive reactance. The electrical circuit shown in Figure 2 can be easily reduced to the equivalent circuit presented in Figure 5. In this circuit, we can calculate the Thevenin equivalent voltage V_{1th} and impedance Z_{1th} by:

$$V_{1th} = \frac{V_{pcc} Z_c}{Z_{tr} + Z_C} \tag{18}$$

$$Z_{1th} = R_{1th} + jX_{1th} = \frac{Z_{tr} Z_c}{Z_{tr} + Z_C} \tag{19}$$

$$Z_C = -jX_c \tag{20}$$

$$Z_{tr} = R_{tr} + jX_{tr} \tag{21}$$

The circuit shown in Figure 5 can be easily reduced to the Thevenin equivalent circuit, where the new Thevenin equivalent voltage V_{th} and impedance Z_{th} can be calculated by:

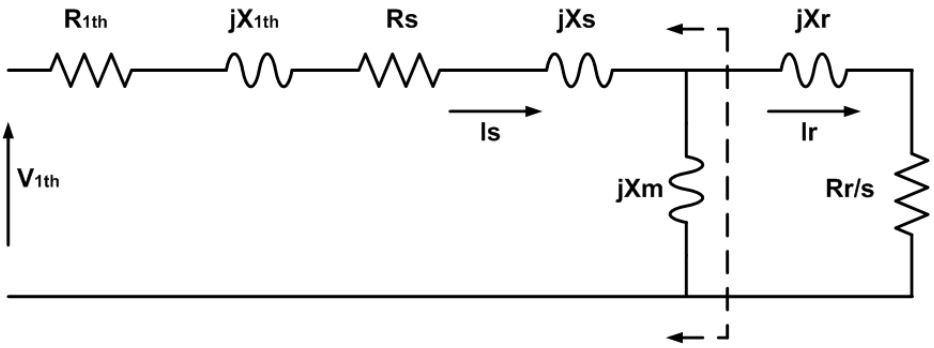

Figure 5. Reduced equivalent circuit of a coupled SCIG with the PCC.

$$V_{th} = \frac{V_{1th} Z_M}{Z_{1th} + Z_S + Z_M} \tag{22}$$

$$Z_{th} = R_{th} + jX_{th} = \frac{(Z_{1th} + Z_S) Z_M}{Z_{1th} + Z_S + Z_M} \tag{23}$$

$$Z_M = jX_m \tag{24}$$

$$Z_S = R_s + jX_s \tag{25}$$

From this equivalent, the magnitude of the rotor current can be determined by:

$$I_r = \frac{V_{th}}{\sqrt{(R_{th} + R_r/s)^2 + (X_{th} + X_r)^2}} \tag{26}$$

and finally, the electrical torque can be calculated by:

$$T_e = {I_r}^2 \frac{R_r}{s} \frac{1}{\omega_s} = \frac{R_r}{s} \frac{1}{\omega_s} \frac{{V_{th}}^2}{(R_{th} + R_r/s)^2 + (X_{th} + X_r)^2} \tag{27}$$

By using Equations (15) and (27), the electric torque T_e *versus* the rotor speed ω_R curve of SCIG can be plotted, as depicted in Figure 6.

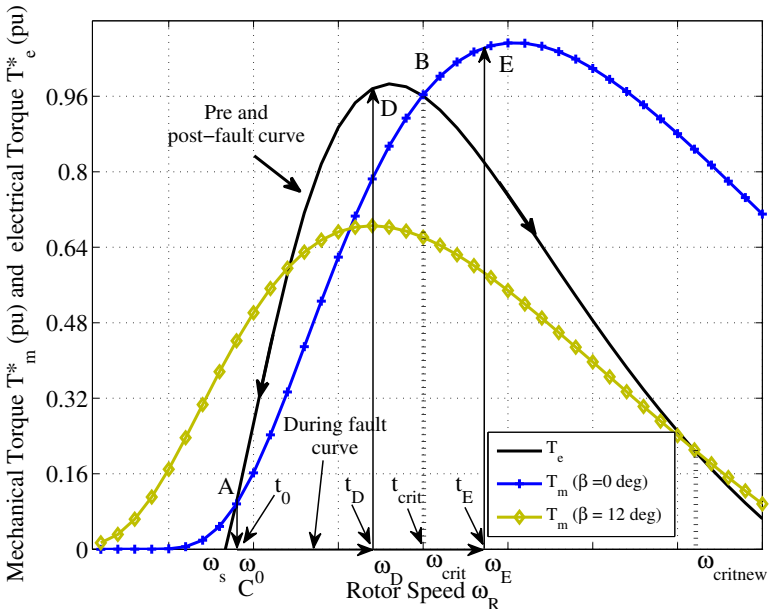

Figure 6. Dynamic stability improvement by increasing the pitch angle value.

The electrical mechanical equilibrium equation of SCIG is in accordance with [12]:

$$\frac{d\omega_R}{dt} = \frac{1}{2H}(T_e - T_m) \tag{28}$$

where H is the inertia constant. By using Equation (28), two equilibrium points can be determined by making $T_e = T_m$ in Equation (27). This leads to,

$$({R_{th}}^2 + (X_{th} + X_r)^2)s^2 + (2R_rR_{th} - R_r\frac{{V_{th}}^2}{T_m})s + {R_r}^2 = 0 \tag{29}$$

Starting from Figure 3, the electrical-mechanical characteristics of SCIG in pre-fault and during fault conditions can be seen in Figure 6. To simplify the visualization, in all cases, the electrical and mechanical torque are multiplied by minus one (-1). In the steady-state condition, the T_e is equal to the $T_m(\beta = 0°)$ at two different rotor speeds ω_0 and ω_{crit}, which are given by the intersection between the two curves. The operating point A is a stable equilibrium point whose rotor speed is denoted as ω_0, whereas the operating point B is unstable, and its rotor speed is denoted as ω_{crit}.

The SCIG is operating initially at point A, which corresponds to ω_0. At this instant (t_0), a fault is applied; the T_e abruptly decreases to zero due to a sudden drop in the V_{pcc}, and the machine operating point is shifted from point A of the pre-fault curve to point C of the during fault (zero) curve. Now, the ω_R starts to increase governed by Equation (28). At instant t_D, the fault is eliminated, and the SCIG operating point changes to D, as shown in Figure 6. As $T_e > T_m$, from Equation (28), the ω_R will decrease, and eventually, the generator will return to its stable equilibrium point A.

If the fault duration is longer and not cleared before time $t = t_{crit}$, ω_R will increase to ω_E, which is larger than ω_{crit}, as shown in Figure 6. If the fault is cleared at this time (t_E), the operating point will

now move to the point E. However, T_e being smaller than T_m, then ω_R will continue to increase, making the system unstable.

Therefore, it is necessary to balance T_m and T_e for enhancing the FRT capability of SCIG. In fact, at the moment of fault clearance, if the ω_{crit} is more than the ω_R, the SCIG will remain stable; otherwise, it will be unstable. By using Equations (29) and (15), one can calculate the steady-state rotor speed ω_0 and the critical rotor speed ω_{crit}; thus, the large-disturbance stability of an SCIG can be determined by analyzing the time response of the rotor speed after the fault application by:

$$\omega_0 = 1 - \frac{b + \sqrt{\Delta}}{2a} \tag{30}$$

$$\omega_{crit} = 1 - \frac{b - \sqrt{\Delta}}{2a} \tag{31}$$

where $a = {R_{th}}^2 + (X_{th} + X_r)^2$, $b = 2R_r R_{th} - R_r \frac{{V_{th}}^2}{T_m}$, $c = {R_r}^2$ and $\Delta = b^2 - 4ac$.

By integrating Equation (28), we get:

$$\int_0^{t_{crit}} dt = \frac{2H}{T_e - T_m} \int_{\omega_0}^{\omega_{crit}} dt \tag{32}$$

If we assume that $T_e - T_m$ remains constant, this leads to:

$$t_{crit} = \frac{2H}{T_e - T_m}(\omega_{crit} - \omega_0) \tag{33}$$

Substituting Equations (31) and (30) in Equation (33), as suggested in [12], finally, the critical clearing time t_{crit} (*i.e.*, the maximum allowed time for WT to remain connected to the grid before becoming unstable) when the grid is subjected to a fault is given by:

$$t_{crit} = a \cdot B \tag{34}$$

where:

$$A = \frac{-2H}{T_m({R_{th}}^2 + (X_{th} + X_r)^2)} \tag{35}$$

$$B = \sqrt{\frac{{R_r}^2}{{T_m}^2}(-4(X_{th} + X_r)^2 {T_m}^2 - (4R_{th}{V_{th}}^2 T_m) + {V_{th}}^4} \tag{36}$$

As we can see from Equations (31) and (34), in terms of the dynamic stability limit considerations, the ω_{crit} and t_{crit} of the WT can be improved by a temporary reduction of T_m, which can be achieved by increasing the value of the pitch angle. Graphically, this is illustrated in Figure 3, *i.e.*, increasing the pitch angle by $\beta = 12°$, as shown in Figure 6, this leads to ω_{crit} varying from its initial value to $\omega_{crit,new}$; thus, the stable operating range is expanded significantly from ω_{crit} to $\omega_{crit,new}$.

4. Hybrid Control Design for a Pitch Angle Controller

In a previous work [26], the authors presented a pitch angle control method and a hybrid controller to adapt the pitch angle in response to different output power for all operating regions of SCIG WT. For the purpose of improving the output power quality performance of the SCIG WT in all operating regions by utilizing the good control capability of fuzzy and PI techniques, a hybrid control strategy is presented in Figure 7, following the approach presented in [26]. When the rotor speed is higher than the base generator speed given by the manufacturer, the β selection Switch 1 moves to β_{PI} input; thus, $\beta_{Ref} = \beta_{Normal} = \beta_{PI}$. On the other hand, the β selection Switch 1 moves to the β_{Fuzzy} input; thus $\beta_{Ref} = \beta_{Normal} = \beta_{Fuzzy}$.

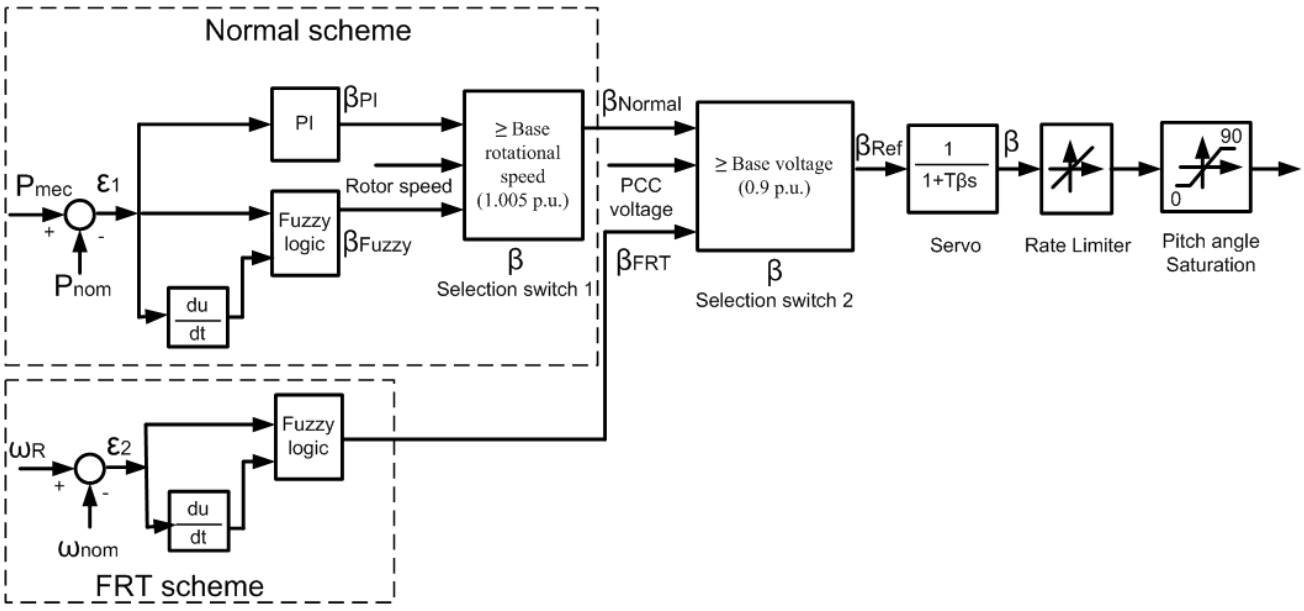

Figure 7. Hybrid pitch angle controller.

However, in [26], the power system stability requirements are not necessarily considered. When a short circuit fault happens in the external grid, the voltage drops, as well as the measured power P_{mec}. The pitch angle control will detect this reduction of output power, and it will try to increase the P_{mec} by keeping β_{Ref} close to zero. This process may result in a higher acceleration of the SCIG and to system instability, if no other action is performed. In this case, alternative input signals to the pitch angle control should be considered.

4.1. FRT Operation

In this paper, this hybrid controller is proposed as a new and simple method to perform the transient stability of SCIG without using any additional equipment. The architecture of the proposed pitch controller is illustrated in Figure 7, which includes the normal and FRT schemes in the enclosed dotted line parts. In this controller, by the coordination of a protective relay system for SCIG WT [35], a sudden voltage sag is quickly detected by the undervoltage relay, which initiates the β selection Switch 2 in Figure 7.

In order to maintain voltage stability, after a short circuit fault, the rotor speed signal ω_R controls the blade angle [36] to avoid the voltage instability related to over-speeding of the SCIG, as shown in Section 2 and in Figure 4. Since the rotor speed can vary in the range of a few percent, it may be useful to implement a fuzzy logic controller (FLC) for the blade angle control system to increase the sensitivity of the error signal ϵ_2, as shown again in Figure 7 [26].

After the PCC voltage decreases below the base voltage (0.9 pu), the pitch angle is changed according to the increase of ω_R, so as to repress the rapid raise of the rotor speed by the discharge of blowing wind energy. By means of this, the T_m can be controlled in order to extend ω_{crit} (Figure 6). As reported in Figure 7, the input control variables to the FLC are the rotor speed error ϵ_2 and its derivative. With any variation of β, the corresponding value of T_m is estimated. If ϵ_2 increases with the last positive derivative, this indicates that the variation of β is continued in the same direction. Otherwise, the negative derivative causes a decrease in ϵ_2, and the direction of search for a suitable β is immediately reversed. In the following, all of the variables are described by using a fuzzy logic language [37].

4.2. Proposed Methodology

FLC has number of design parameters, which give great flexibility for the designer to make an effective controller for the required system. In order to design the FLC, the following fundamental design steps for an FLC are employed and refer to [26]. The fuzzy system structure has three basic blocks, which include fuzzification (FI), decision-making logic (DML), defuzzification (DFI) and knowledge base (KB). Figure 7 plots the block diagram of FLC FRT scheme, where $\epsilon_2 = (\omega_R - \omega_{nom})/\omega_{nom}$, and its derivative are fuzzified using the Gaussian and the generalized bell membership function, respectively (Figure 8), for sending to FLC to generate a suitable β, which is characterized by the triangular membership function according to Figure 9. Then, the DML gives a fuzzy set utilizing the rule base KB, as reported in [26]. Lastly, the DFI is applied to the fuzzy sets produced by the DML in order to convert the fuzzy set into a numerical value by equation in [38]:

$$y(x) = \frac{\sum_j^N w_j \mu_j(x)}{\sum_j^N \mu_j(x)} \tag{37}$$

where $y(x)$ is the output reference pitch angle, w_j is the weight corresponding to a given output fuzzy set, $\mu_j(x)$ is the degree of the fuzzy rule and x is the input vector.

In this work, a 9×3 FLC is implemented. The $\epsilon_2 = (\omega_R - \omega_{nom})/\omega_{nom}$, and its derivative input variable has nine and three fuzzy sets, respectively. Similarly, the β output has nine membership functions. The notations of the membership functions are: large negative (LN), medium negative (MN), small negative (SN), negative (N), zero (ZO), positive (P), small positive (SP), medium positive (MP) and large positive (LP).

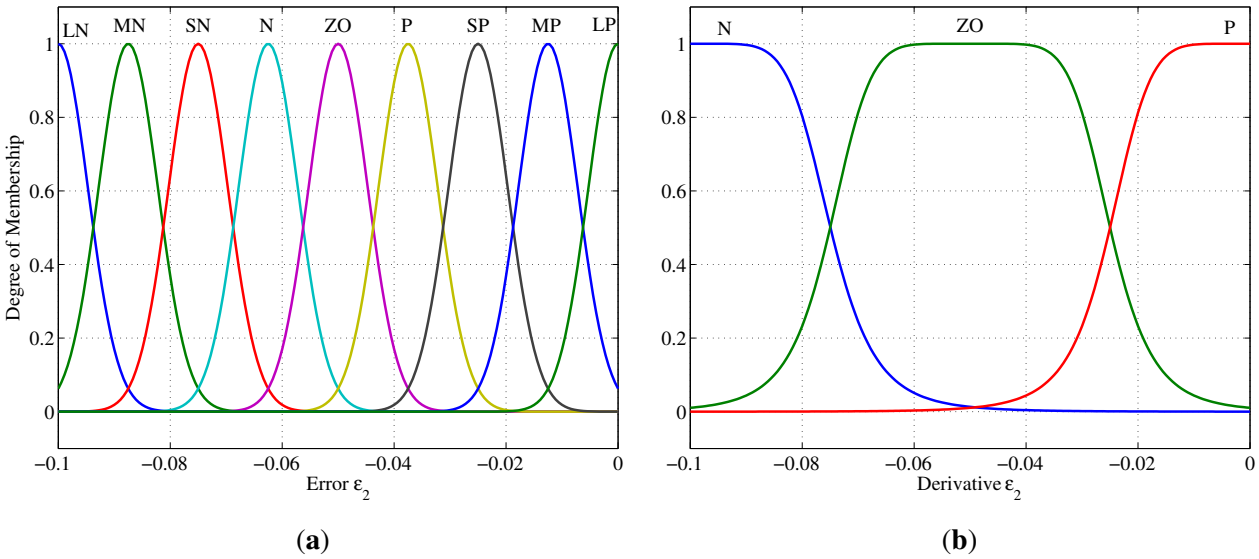

Figure 8. Input fuzzy set for rotor speed error (**a**) and its derivative (**b**).

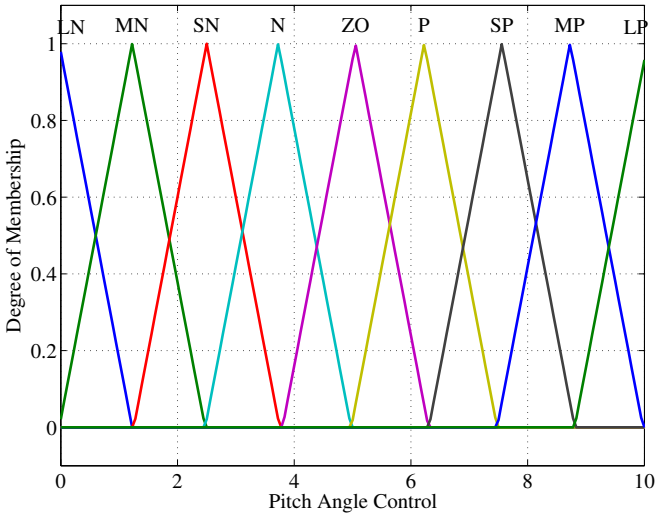

Figure 9. Output fuzzy set for pitch angle control.

In order to obtain power smoothing and FRT for SCIG WT, the coordination with switching logic in the hybrid controller is desired. The normal mode and FRT mode are activated by the switching logic system, which coordinates the pitch controller in Figure 7. The proposed methodology is shown in Figure 10. If PCC voltage dip beginning is detected, the protection system switches the FRT scheme pitch control action with the input signal of the SCIG rotor speed. Otherwise, the normal scheme pitch control is carried out with the output power as the input signal.

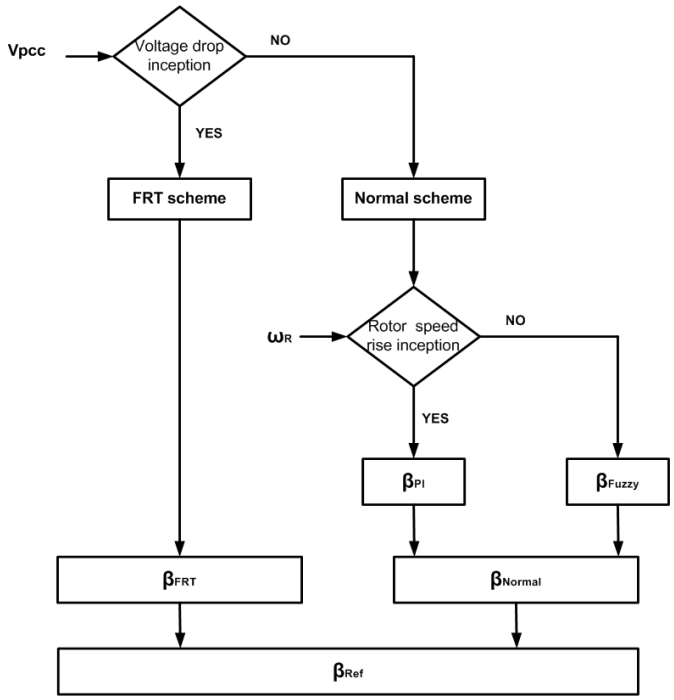

Figure 10. Flow chart to obtain the normal fault ride-through (FRT) mode in the hybrid controller.

5. Simulation Results and Discussion

In this section, we compare the pitch angle control performance of the proposed hybrid controller *versus* the conventional PI controller. The considered pitch rate capability (8 deg/s to ramp both up and down) is taken from [39,40], which present the specifications of a representative utility-scale large power turbine now known as the "NREL offshore 5-MW baseline wind turbine". This model has been used as a reference by many research teams to standardize baseline offshore wind turbine specifications.

In this work, the performance of the proposed control system was evaluated with MATLAB/Simulink for a 3-MW SCIG-based WT. The system simulated is the same configuration as the one shown in Figure 1, where SCIG is connected directly to two 33-kV, 10-km parallel power lines at the point of common connection (PCC). The SCIG and network parameters are given in Table 1. Some data about SCIG and the wind speed profile are taken from [26]: in particular, the real turbulent wind speed and its relative measured value (Figure 11) have been used to test the controllers and to assess the performance of the SCIG.

Before illustrating the contribution of the FRT control system to the characteristic operation of an SCIG WT system in the transient state, the SCIG dynamic behavior with a normal control system is presented in the following.

Table 1. Grid-connected wind turbine parameters.

Parameters	Value	Unit
SCIG:		
Rated power	3	MW
Rated speed	12	m/s
Cut in wind speed	5	m/s
Cut out wind speed	19	m/s
Rated voltage	690	V
Frequency	50	Hz
R_s	0.00488	pu
R_r	0.00549	pu
L_{ls}	0.09241	pu
L_{lr}	0.09955	pu
L_m	3.95279	pu
Q_{pf}	200	kvar
Grid power source:		
Rated capacity	12/110	MVA/kV
R	0.00796	pu
X	0.0796	pu
R/X	0.1	

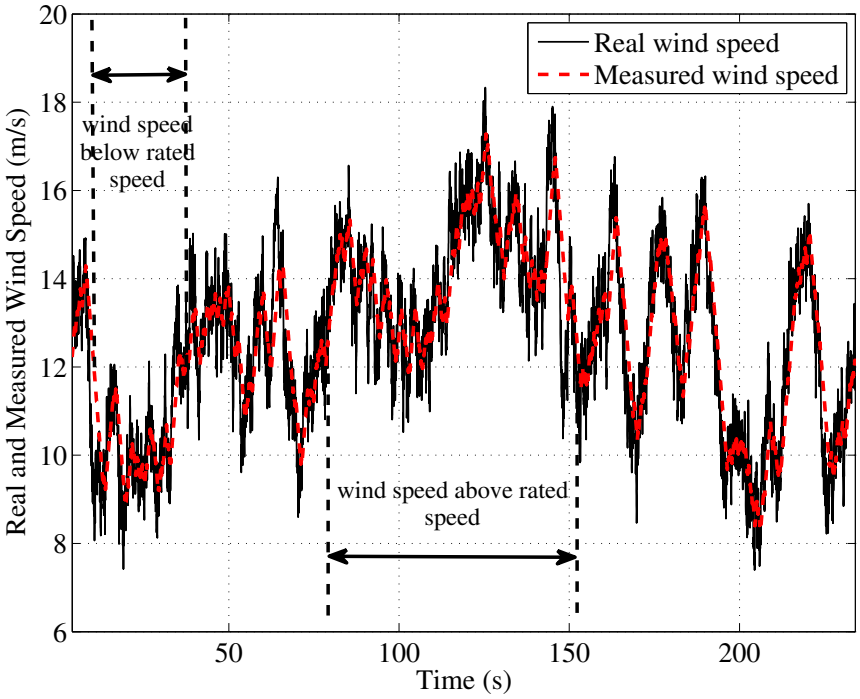

Figure 11. Real and measured wind speed profile.

5.1. Comparison in Terms of SCIG Dynamic Behavior during Normal Operation

As reported in [26], the proposed hybrid control system is used to improve the quality and the amplitude of SCIG WT output power. In order to clarify the effect of the proposed method [41], several performance indexes that present the performance of output power, namely P_{eff} and P_{sm}, are shown as:

$$P_{eff} = \int_0^T |P_{mec}| dt \tag{38}$$

$$P_{sm} = \int_0^T |\Delta P_{mec}| dt \tag{39}$$

where ΔP_{mec} denotes the real power deviation of SCIG WT and T is the simulation time. If P_{eff} in Equation (38) is large, the efficiency of SCIG WT is good. If P_{sm} in Equation (39) is small, the output power fluctuation is small enough to guarantee an appropriate smoothing of the output power.

Figures 12 and 13 show, respectively, the steady-state active power P_{mec}, P_{eff} and P_{sm} in three different cases for the pitch angle control: using a conventional PI, using a fuzzy controller and with our proposed hybrid controller. Obviously, the output power fluctuates greatly because of the difference of the pitch angle. The proposed method with the hybrid controller gives a smoothed output, and there is no large effect on the amplitude by a suitable pitch angle. If compared with the conventional method, P_{eff} of the proposed method drops to about 9%, as shown in Figure 13a. In the meantime, the drop of the fuzzy controller in the pitch angle control is about 31%. Since the purpose of this work is smoothing the output power using pitch angle control, a drop in the output power cannot be avoided. Because the pitch angle is fixed at 0° in the cut-in wind speed region to the rated wind speed region, P_{eff} of conventional method is maximum. However, if the pitch angle is fixed, input torque T_m cannot be controlled, and this results in increasing P_{sm}, while the proposed method is able to limit this effect, as shown in Figure 13b.

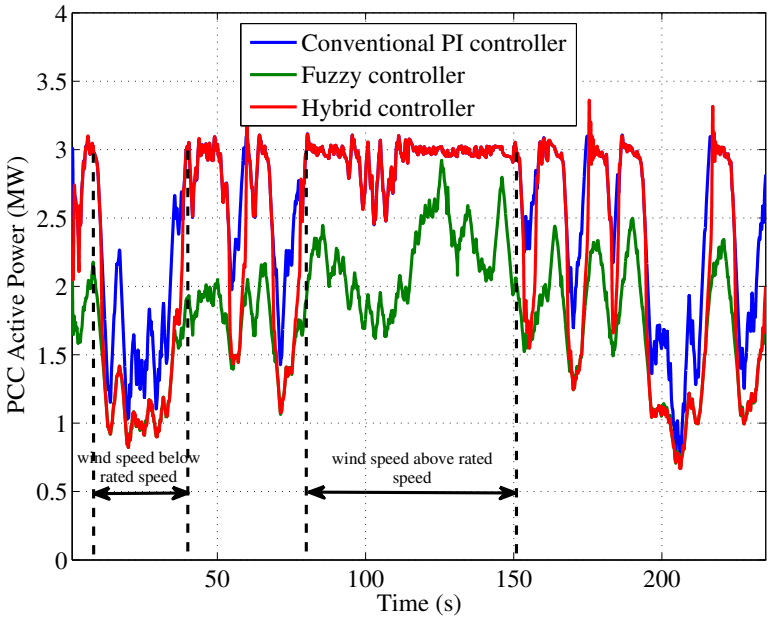

Figure 12. Active power at PCC.

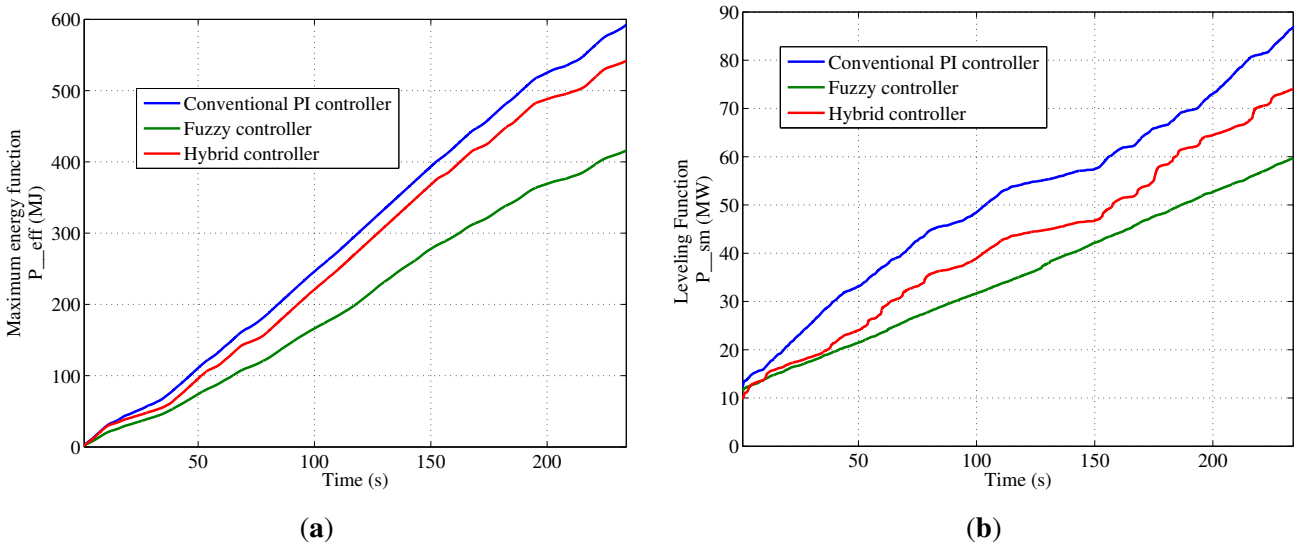

(**a**) (**b**)

Figure 13. Efficiency energy (**a**) and smoothing function (**b**).

5.2. Comparison in Terms of SCIG Fault Ride-Through Enhancement

As can be seen in Figure 1, the fault event is a three-phase to ground fault at the point Fnear the SCIG WT of one of two parallel lines. Simulations are carried out considering two cases (with reference to Figure 12): (1) wind speed higher than the rated speed; and (2) wind speed lower than the rated speed.

5.2.1. Wind Speed above the Rated Speed Case

In this case, the permanent three-phase fault occurs at $t = 90$ s, and it is cleared by the breakers after 150 ms. A comparison of the SCIG PCC voltage, SCIG rotor speed, SCIG pitch angle, SCIG mechanical torque, SCIG electrical torque and SCIG active power for the two controllers is shown in Figure 14. As reported in Figure 14a, the PCC voltage with the hybrid controller has regained its pre-fault value, while the one with the conventional controller has collapsed. It should be noted that the large increase of pitch angle, shown in Figure 14c, causes the mechanical torque decrease, as shown in Figure 14d; thus, the rotor speed boosts the PCC voltage at fault clearance. Figure 14e shows a comparison of the electrical torque for the two cases during the fault event. The SCIG rotor speed and the PCC active power gradually get back to their nominal values after the fault in the hybrid system, whereas the conventional system exhibits unstable responses, as shown in Figure 14b,f.

Obviously, when the rotor speed becomes higher than the safe speed from $t = 90$ s (Figure 14b), the proposed controller increases the pitch angle continuously (Figure 14c), and simultaneously, the mechanical torque decreases (Figure 14d). This process lasts until the rotor speed comes back to the safe value at $t = 91$ s.

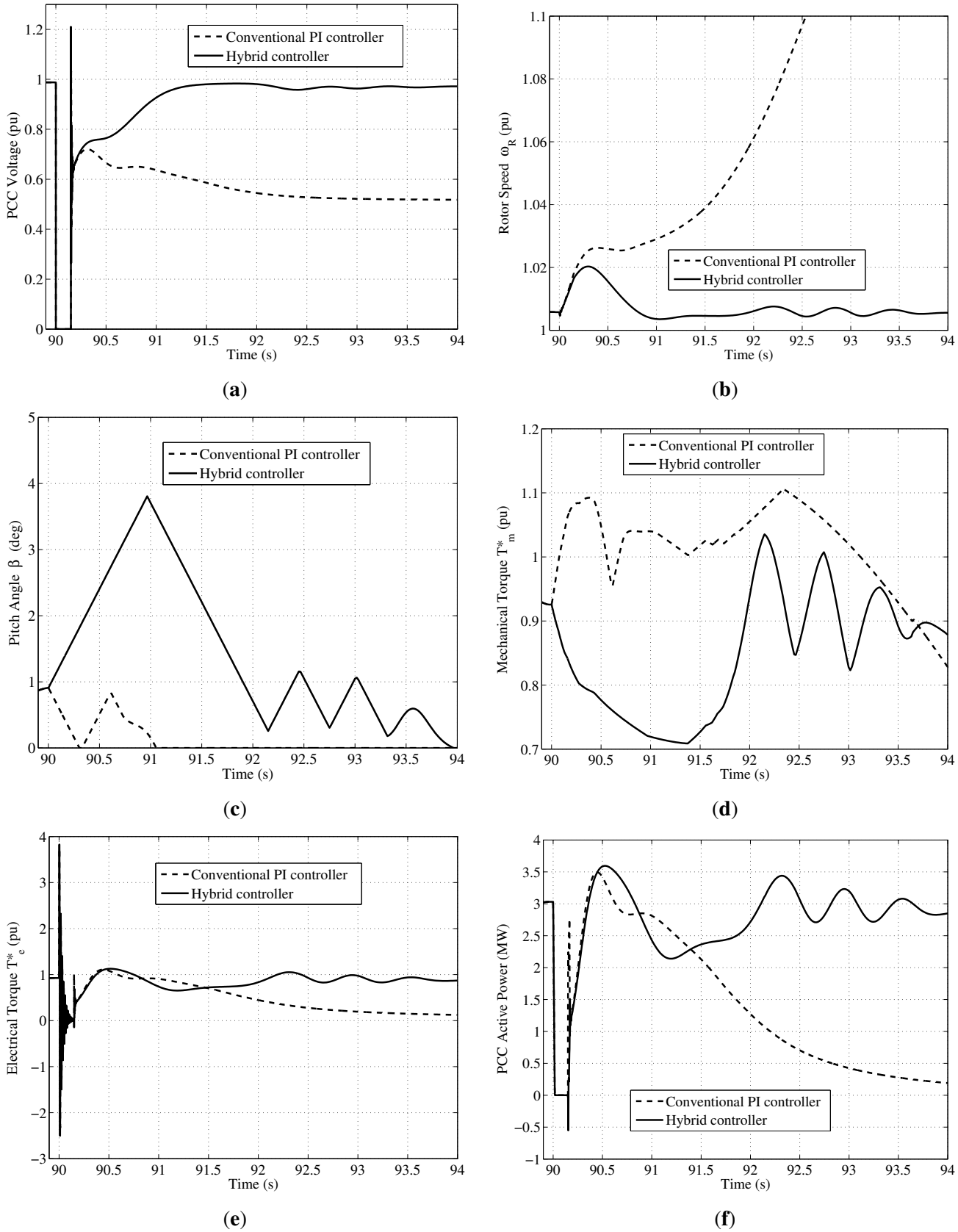

Figure 14. Responses of SCIG on the FRT scheme with wind above the rated speed: PCC voltage (**a**); rotor speed (**b**); pitch angle (**c**); mechanical torque (**d**); electrical torque (**e**); and active power (**f**).

5.2.2. Wind Speed below the Rated Speed Case

In this case, fault occurs at $t = 25$ s, and it is cleared by the breakers after 150 ms. In both situations with the hybrid controller and conventional controller, the wind generator can be stabilized (Figure 15), but it can be noted that the response of the SCIG PCC voltage and SCIG rotor speed recovers faster to their rated value with the hybrid controller. The PCC voltage recovers to 0.9 p.u.within 550 ms, and the rotor speed of SCIG comes back to the pre-fault value within 650 ms with the conventional PI controller. However, if the hybrid controller is used, the PCC voltage recovers to 0.9 p.u. within 450 ms, where the rotor speed comes back to its pre-fault value within 550 ms, as shown in Figure 15a,b.

Figure 15c,d shows the relationship between the pitch angle and the mechanical torque. It can be concluded that a change of pitch angle that depends on the size of ϵ_2 (as defined in Figure 7) will significantly affect the magnitude of the mechanical torque. Figure 15e,f shows the electrical torque of WT and active power at the point of connection that is restored to its normal operating condition after a considerable time.

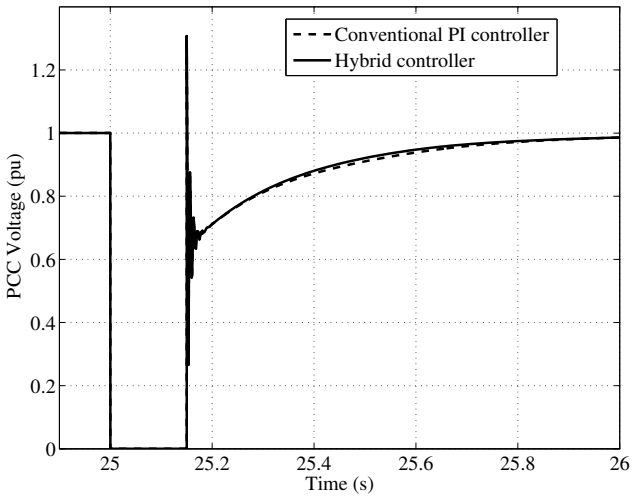

(**a**)

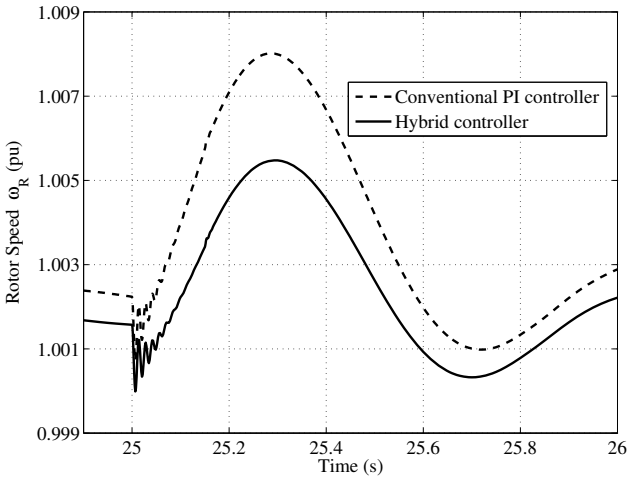

(**b**)

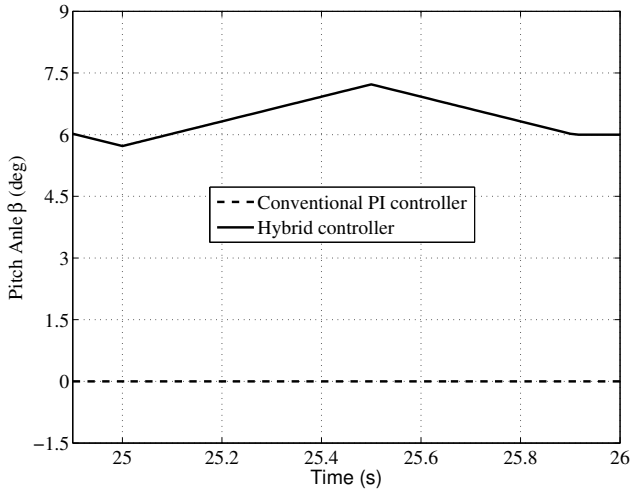

(**c**)

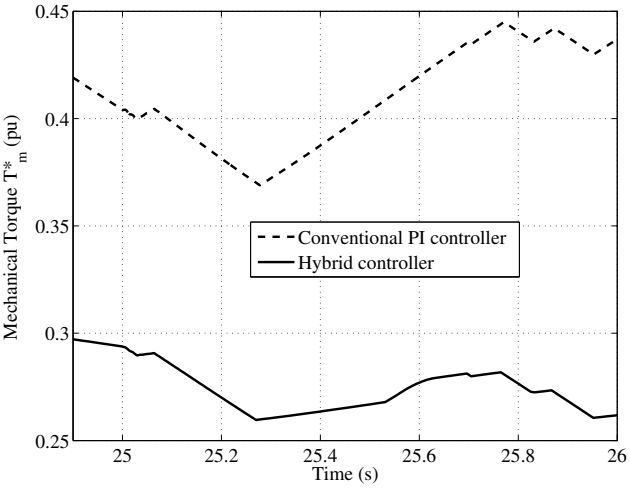

(**d**)

Figure 15. *Cont.*

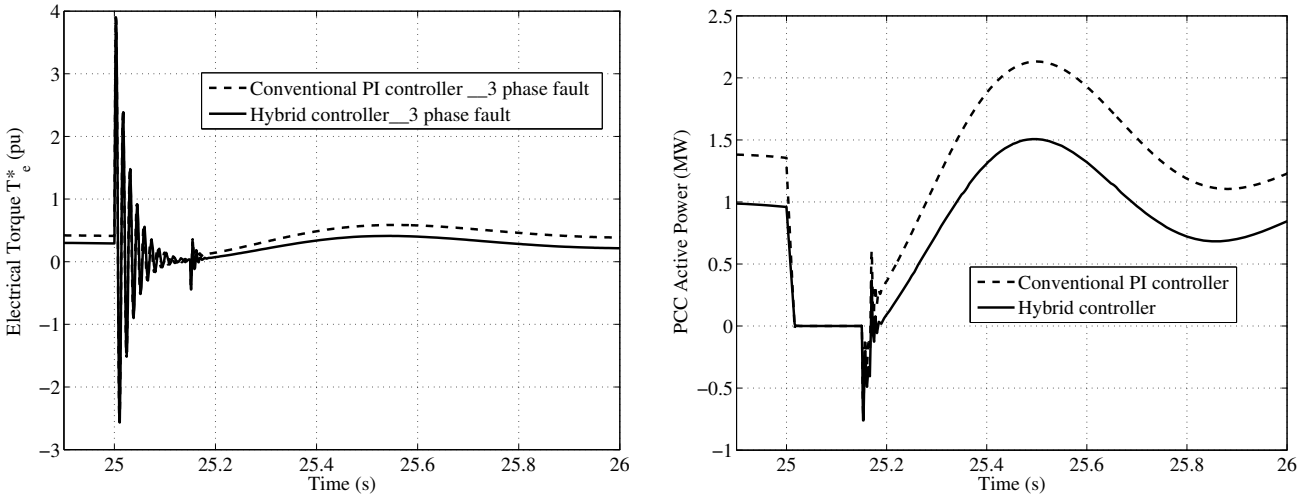

(**e**) (**f**)

Figure 15. Responses of SCIG on the FRT scheme with wind below the rated speed: PCC voltage (**a**); rotor speed (**b**); pitch angle (**c**); mechanical torque (**d**); electrical torque (**e**); and active power (**f**).

6. Conclusions

In this work, a comparative analysis of a pitch angle controller for SCIG WT has been presented, by considering conventional PI and a hybrid PI-fuzzy technique, both in a normal and an FRT scheme, considering in particular the performance of output power leveling, as well as the SCIG transient.

Based on the analytic approach of the physical equivalent circuit of the SCIG WT from the PCC, some key factors that may affect SCIG transient stability were investigated. Moreover, the relationship between mechanical torque and electrical torque was performed under different pitch angle conditions. This approach is important to expand operating limitations in order to guarantee SCIG WT connected to a grid during a three-phase short circuit.

The pitch control system is an inexpensive, but slow solution for SCIG WT power fluctuation minimization and its stabilization in the case of permanent fault. Simulations have shown that the quality, amplitude, as well as FRT capability of an SCIG wind system can be enhanced with the proposed hybrid control system.

It was found that, if a fixed-speed induction generator wind turbine is equipped with a suitable controller, it can improve the power quality, efficiency, as well as satisfy the low voltage ride-through capability, which are the main disadvantages of a wind farm furnished with this type of generator. Therefore, this controller configuration might be an effective solution to considerable increase future SCIG WT performance, in terms of simplicity, reliability, low weight and low maintenance cost.

Author Contributions

In this research activity, all of the authors were involved in the data analysis and processing phase, simulation, results analysis and discussion and the manuscript preparation. All authors have approved the submitted manuscript.

Conflicts of Interest

The authors declare no conflict of interest.

References

1. Golovanov, N.; Lazaroiu, G.; Roscia, M.; Zaninelli, D. Power Quality analysis in Renewable Energy Systems Supplying Distribution Grids. *Measurements* **2013**, *7*, 6–95.
2. Duong, M.Q.; Ogliari, E.; Grimaccia, F.; Leva, S.; Mussetta, M. Hybrid model for hourly forecast of photovoltaic and wind power. In Proceedings of the 2013 IEEE International Conference on Fuzzy Systems (FUZZ), Hyderabad, India, 7–10 July 2013; pp. 1–6.
3. Cheng, M.; Zhu, Y. The state of the art of wind energy conversion systems and technologies: A review. *Energy Convers. Manag.* **2014**, *88*, 332–347.
4. Sava, G.N.; Costinas, S.; Golovanov, N.; Leva, S.; Duong, M.Q. Comparison of active crowbar protection schemes for DFIGs wind turbines. In Proceedings of the 2014 IEEE 16th International Conference on Harmonics and Quality of Power (ICHQP), Bucharest, Romania, 25–28 May 2014; pp. 669–673.
5. Duong, M.Q.; Le, K.H.; Grimaccia, F.; Leva, S.; Mussetta, M.; Zich, R. Comparison of power quality in different grid-integrated wind turbines. In Proceedings of the 2014 IEEE 16th International Conference on Harmonics and Quality of Power (ICHQP), Bucharest, Romania, 25–28 May 2014; pp. 448–452.
6. Holdsworth, L.; Wu, X.; Ekanayake, J.; Jenkins, N. Comparison of fixed speed and doubly-fed induction wind turbines during power system disturbances. *IEEE Proc. Gener. Trans. Distrib.* **2003**, *150*, 343–352.
7. Akhmatov, V.; Knudsen, H.; Hejde Nielsen, A.; Kaas Pedersen, J.; Kjølstad Poulsen, N. Modelling and transient stability of large wind farms. *Int. J. Electr. Power Energy Syst.* **2003**, *25*, 123–144.
8. Rahimi, M.; Parniani, M. Dynamic behavior and transient stability analysis of fixed speed wind turbines. *Renew. Energy* **2009**, *34*, 2613–2624.
9. Samuelsson, O.; Lindahl, S. On speed stability. *Power Syst. IEEE Trans.* **2005**, *20*, 1179–1180.
10. Kundur, P.; Paserba, J.; Ajjarapu, V.; Andersson, G.; Bose, A.; Canizares, C.; Hatziargyriou, N.; Hill, D.; Stankovic, A.; Taylor, C.; *et al*. Definition and classification of power system stability IEEE/CIGRE joint task force on stability terms and definitions. *Power Syst. IEEE Trans.* **2004**, *19*, 1387–1401.
11. Lin, F.J.; Tan, K.H.; Fang, D.Y. Squirrel-cage induction generator system using hybrid wavelet fuzzy neural network control for wind power applications. *Neural Comput. Appl.* **2014**, *26*, 911–928.

12. Grilo, A.P.; Mota, A.; Mota, L.T.M.; Freitas, W. An analytical method for analysis of large-disturbance stability of induction generators. *Power Syst. IEEE Trans.* **2007**, *22*, 1861–1869.
13. Li, H.; Zhao, B.; Yang, C.; Chen, H.; Chen, Z. Analysis and estimation of transient stability for a grid-connected wind turbine with induction generator. *Renew. Energy* **2011**, *36*, 1469–1476.
14. Amutha, N.; Kalyan Kumar, B. Improving fault ride-through capability of wind generation system using DVR. *Int. J. Electr. Power Energy Syst.* **2013**, *46*, 326–333.
15. Pedra, J.; Corcoles, F.; Monjo, L.; Bogarra, S.; Rolan, A. On fixed-speed WT generator modeling for rotor speed stability studies. *Power Syst. IEEE Trans.* **2012**, *27*, 397–406.
16. Obando-Montano, A.F.; Carrillo, C.; Cidras, J.; Diaz-Dorado, E. A STATCOM with Supercapacitors for Low-Voltage Ride-Through in Fixed-Speed Wind Turbines. *Energies* **2014**, *7*, 5922–5952.
17. Lahaçani, N.A.; Aouzellag, D.; Mendil, B. Static compensator for maintaining voltage stability of wind farm integration to a distribution network. *Renew. Energy* **2010**, *35*, 2476–2482.
18. Qiao, W.; Harley, R.G.; Venayagamoorthy, G.K. Coordinated reactive power control of a large wind farm and a STATCOM using heuristic dynamic programming. *Energy Convers. IEEE Trans.* **2009**, *24*, 493–503.
19. Jayashri, R.; Kumudini Devi, R. Effect of tuned unified power flow controller to mitigate the rotor speed instability of fixed-speed wind turbines. *Renew. energy* **2009**, *34*, 591–596.
20. Zamani, M.; Fathi, S.; Riahy, G.; Abedi, M.; Abdolghani, N. Improving Transient Stability of Grid-Connected Squirrel-Cage Induction Generators by Plugging Mode Operation. *Energy Convers. IEEE Trans.* **2012**, *27*, 707–714.
21. Freitas, W.; Morelato, A.; Xu, W. Improvement of induction generator stability using braking resistors. *Power Syst. IEEE Trans.* **2004**, *19*, 1247–1249.
22. Nunes, M.V.; Peas Lopes, J.; Zurn, H.H.; Bezerra, U.H.; Almeida, R.G. Influence of the variable-speed wind generators in transient stability margin of the conventional generators integrated in electrical grids. *Energy Convers. IEEE Trans.* **2004**, *19*, 692–701.
23. Croft, W.; Hartley, R. Improving transient stability by use of dynamic braking. *Power Appar. Syst. Part III Trans. Am. Inst. Electr. Eng.* **1962**, *81*, 17–24.
24. Causebrook, A.; Atkinson, D.J.; Jack, A.G. Fault ride-through of large wind farms using series dynamic braking resistors (March 2007). *Power Syst. IEEE Trans.* **2007**, *22*, 966–975.
25. Machowski, J.; Bialek, J.; Bumby, J. *Power System Dynamics: Stability and Control*; John Wiley & Sons: Hoboken, NJ, USA, 2011.
26. Duong, M.Q.; Grimaccia, F.; Leva, S.; Mussetta, M.; Ogliari, E. Pitch angle control using hybrid controller for all operating regions of SCIG wind turbine system. *Renew. Energy* **2014**, *70*, 197–203.
27. Fernandez, L.; Garcia, C.; Saenz, J.; Jurado, F. Equivalent models of wind farms by using aggregated wind turbines and equivalent winds. *Energy Convers. Manag.* **2009**, *50*, 691–704.
28. Duong, M.Q.; Grimaccia, F.; Leva, S.; Mussetta, M.; Sava, G.; Costinas, S. Performance analysis of grid-connected wind turbines. *UPB Sci. Bull. Ser. C* **2014**, *76*, 169–180.

29. Duong, M.Q.; Grimaccia, F.; Leva, S.; Mussetta, M.; Zich, R. Improving LVRT characteristics in variable-speed wind power generation by means of fuzzy logic. In Proceedings of the 2014 IEEE International Conference on Fuzzy Systems (FUZZ-IEEE), Beijing, China, 6–11 July 2014; pp. 332–337.
30. Haque, M. Evaluation of power flow solutions with fixed speed wind turbine generating systems. *Energy Convers. Manag.* **2014**, *79*, 511–518.
31. Eminoglu, U.; Ayasun, S. Modeling and Design Optimization of Variable-Speed Wind Turbine Systems. *Energies* **2014**, *7*, 402–419.
32. Strzelecki, R.; Benysek, G. *Power Electronics in Smart Electrical Energy Networks*; Springer: London, UK, 2008.
33. Trudnowski, D.J.; Gentile, A.; Khan, J.M.; Petritz, E.M. Fixed-speed wind-generator and wind-park modeling for transient stability studies. *Power Syst. IEEE Trans.* **2004**, *19*, 1911–1917.
34. Zhang, J.; Yin, Z.; Xiao, X.; Di, Y. Enhancement voltage stability of wind farm access to power grid by novel SVC. In Proceedings of the 4th IEEE Conference on Industrial Electronics and Applications, 2009 (ICIEA 2009), Xi'an, China, 25–27 May 2009; pp. 2262–2266.
35. Thet, A.K.; Saitoh, H. Pitch control for improving the low-voltage ride-through of wind farm. In Proceedings of the Transmission Distribution Conference Exposition: Asia and Pacific, Seoul, Korea, 26–30 October 2009; pp. 1–4.
36. You, R.; Barahona, B.; Chai, J.; Cutululis, N.A. A Novel Wind Turbine Concept Based on an Electromagnetic Coupler and the Study of Its Fault Ride-through Capability. *Energies* **2013**, *6*, 6120–6136.
37. Aissaoui, A.G.; Tahour, A.; Essounbouli, N.; Nollet, F.; Abid, M.; Chergui, M.I. A Fuzzy-PI control to extract an optimal power from wind turbine. *Energy Convers. Manag.* **2013**, *65*, 688–696.
38. Abe, S. Fuzzy function approximators with ellipsoidal regions. *Syst. Man Cybern. Part B Cybern. IEEE Trans.* **1999**, *29*, 654–661.
39. Jonkman, J.M.; Butterfield, S.; Musial, W.; Scott, G. *Definition of a 5-MW Reference Wind Turbine for Offshore System Development*; National Renewable Energy Laboratory: Golden, CO, USA, 2009.
40. Laks, J.; Dunne, F.; Pao, L. Feasibility studies on disturbance feedforward techniques to improve load mitigation performance. *Contract* **2010**, *303*, 275–3000.
41. Viveiros, C.; Melicio, R.; Igreja, J.; Mendes, V. Performance assessment of a wind energy conversion system using a hierarchical controller structure. *Energy Convers. Manag.* **2015**, *93*, 40–48.